AN UPDATED POINT DESIGN FOR HEAVY ION FUSION

S.S. Yu[1], W.R. Meier[2], R.P. Abbott[2], J.J. Barnard[2], T. Brown[3], D.A. Callahan[2], C. Debonnel[1,4], P. Heitzenroeder[3], J.F. Latkowski[2], B.G. Logan[1], S.J. Pemberton[4], P.F. Peterson[4], D.V. Rose[5], G-L. Sabbi[1], W.M. Sharp[2], D.R. Welch[5]

1. Lawrence Berkeley National Laboratory
One Cyclotron Rd., Bldg 47, Berkeley, CA 94720
ssyu@lbl.gov (510) 486-5477
2. Lawrence Livermore National Laboratory, Livermore, CA
3. Princeton Plasma Physics Laboratory, Princeton, NJ
4. University of California, Berkeley, CA
5. Mission Research Corporation, Albuquerque, NM

ABSTRACT

An updated, self-consistent point design for a heavy ion fusion (HIF) power plant based on an induction linac driver, indirect-drive targets, and a thick liquid wall chamber has been completed. Conservative parameters were selected to allow each design area to meet its functional requirements in a robust manner, and thus this design is referred to as the Robust Point Design (RPD-2002). This paper provides a top-level summary of the major characteristics and design parameters for the target, driver, final focus magnet layout and shielding, chamber, beam propagation to the target, and overall power plant.

I. INTRODUCTION

Significant progress has been made in recent years on all aspects of heavy ion fusion (HIF) including target design, driver optimizations, driver/chamber interface and many aspects of thick liquid wall chambers. This study describes an integrated heavy-ion fusion power plant design that is self consistent and based on the current best understanding of target physics, accelerator physics, beam propagation and focusing, final focus magnets design and shielding, and chamber dynamics. More details are given in other papers in these proceedings [1-4]. The key goal of this Robust Point Design (RPD) is to provide confidence in the scientific and technical viability of heavy ion fusion (HIF). The design process has selected conservative parameter values, which have allowed each design area to meet its functional requirements in a robust manner. The current RPD is not optimized, but each design team has identified opportunities for design optimization to improve integrated system performance, reliability, and economics. Future iterations of the RPD will integrate the results of new research on phenomena identified to be of importance to the integrated system performance and will identify design modifications that can lead to reductions in system capital and operating costs.

II. TARGET

The chosen target design is a modified version of the distributed radiator target (DRT), which has proven to be a robust, flexible design [5,6,7]. Different versions of this target have been shown to allow longer-range ions [6], different ion stopping profiles [7], and smaller case-to-capsule ratios [7]. For the point design, a further modification of the target was made to accommodate illumination from an array of beams with a maximum extent from centerline of 24 degrees (rather than 12 degrees in the previous version) [8]. This change was needed to accommodate the number of beams together with the magnet and shielding requirements for the RPD. This "large-angle distributed radiator target" (illustrated in Fig. 1) is driven by ion beams that enter in four cones at angles of 6, 12, 18 and 24 degrees. Target physics considerations (i.e. radiation symmetry) require that the beams in the early part of the pulse shape come in at the shallowest angles.

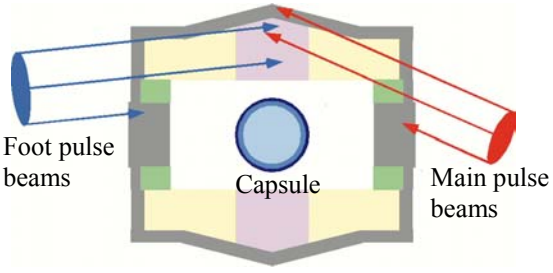

Fig. 1. Large-angle distributed radiator target

Two beneficial side effects came from this requirement. First, the shallow angle foot beams can have a 30% larger beam spot size than the large angle main pulse beams (2.3 mm vs. 1.8 mm). This is helpful for beam focusing since the foot beams do not benefit from the extra neutralizing plasma near the target created by photoionization. Second, the difference in the ion kinetic energy between foot and main pulse beams was reduced (3.3 GeV foot and 4 GeV main versus 3 GeV foot and 4 GeV main) due to the longer path length in the converters for the main pulse beams.

The target requires a specific temporal pulse shape to launch the series of four shocks that compress and heat the capsule. The final focus configuration, in contrast, is most straightforwardly designed using pulses that have a nearly flattop current profile. To accomplish this, a new pulse shape, made up of five "lego blocks" appropriately stacked and timed, was designed (see Fig. 2).

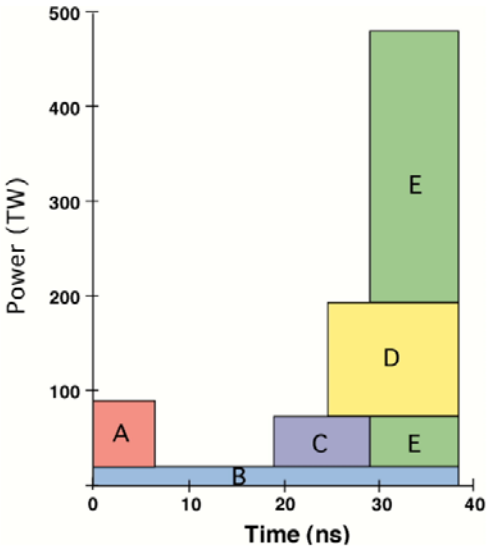

Fig. 2. Pulse shape delivered to the target is made up of five separate blocks with different powers and durations.

To meet the pulse shaping requirements, the present design uses 48 foot-pulse beams with ion kinetic energy of 3.3 GeV (1.76 MJ total) and 72 main-pulse beams with ion energy of 4.0 GeV (5.25 MJ total). Key parameters for the foot and main pulse beams at the target are shown in Table I. Each block uses a minimum of 16 beams (8 from each side) to provide azimuthally symmetric target heating [3]. Based on integrated two-dimensional Lasnex calculations for the large angle DRT and allowances for effects of this new pulse shape configuration (which was developed with 1D modeling), we estimate a target yield of 400 MJ with a total beam energy of 7.0 MJ for a target gain of 57.

Table I. Beam and Pulse Shape Requirements

Block	No. of Beams	Power, TW	Pulse width, ns	Energy, MJ
A (foot)	16	70	6.5	0.46
B (foot)	16	20	38.3	0.77
C (foot)	16	53	10.1	0.54
D (main)	24	120	13.7	1.64
E (main)	48	388	9.3	3.61

III. DRIVER

As indicated above, the target requirements are met with a 120-beam accelerator providing a total of 7.0 MJ to the target. The basic accelerator parameters are obtained from the systems code IBEAM [9,10], which calculates a self-consistent model of a multi-beam induction accelerator. (See illustration of beam configuration in Ref. 3.) The code calculates a model of the source and injector, assuming space-charge limited injection from a Bismuth ion source based on an arc discharge in a hot Bismuth vapor [11]. Beam transport equations are used to calculate the properties of the multiple-beam superconducting magnet arrays. The array of beam lines thread a sequence of induction cores which provide the energy increments to the beam, until the full energy of the foot beams are met. At that point, the foot beams no longer thread the induction cores, whereas the main pulse beams continue to pass through induction cores until their full energy is obtained. Both sets of beams are transported in drift compression sections, after which they pass through the set of final focus magnets, and are finally transported through the fusion chamber to reach the target with the required timing. The detail of the drift compression section layout has yet to be worked out. The driver efficiency at 6 Hz is 38%, and the total length is 2.9 km. Other key driver design parameters are summarized in Table II at three different locations: exit from injector, where the foot pulse beams reach their final energy of 3.3 GeV and where the main pulse beams reach their final energy of 4.0 GeV.

Previous driver systems studies held the charge per beam equal so that all beams were identical at any location inside the induction accelerator. The present concept, however, varies the charge per beam (within a factor of two) in order to meet the target pulse shape requirements with a sequence of different power beams. This can be achieved by maintaining the same quad focusing strength for all channels within a given array but allowing fill factors to vary with the beam charge. Thus, in our system model of the driver, the quads are sized to handle the beams with the highest line charge density

(Block E in Table I) with all the other beams under-filling the bore to some degree.

Table II. Driver Design Parameters at Injection, End of Acceleration for Foot and Main Beam

	Along Accelerator		
	Injector Exit	Foot Final	Main Final
Ion energy, GeV	0.0016	3.3	4.0
Pulse duration, μs	30	0.2	0.2
Ion speed/light speed	0.004	0.18	0.20
Pulse length, m	36.5	10.9	12.0
Beam current, A*	0.63	94	94
Beam radius, cm*	3.8	1.9	1.9
Bore radius, cm	5.3	2.9	2.9
Field gradient, T/m	62	106	106
Core inner radius, m	1.29	0.77	0.62
Core build, m	0.48	0.47	0.47
Quad Occupancy, %	0.75	0.090	0.075
Half lattice period, m	0.30	3.83	4.43
Acc. gradient, MV/m	0.026	1.5	1.5
Dist. from injector, km	0	2.39	2.86
*For maximum current beams (block E)			

IV. FINAL FOCUS SYSTEM

Optimizing the set of magnets that bring each beam to a focus places a number of constraints on the system. The total angle subtended by each beamline viewed from the target must remain small (<~ 5.4 degrees) so that the entire array of quads also subtends a small angle (24 degrees) set by target requirements. Figure 3 illustrates the integrated design [1]. The magnetic field strengths of the superconducting windings must remain below approximately 7 T in the last focusing quadrupole, so that NbTi (with its favorable room-temperature annealing characteristics relative to Nb_3Sn) may be used.

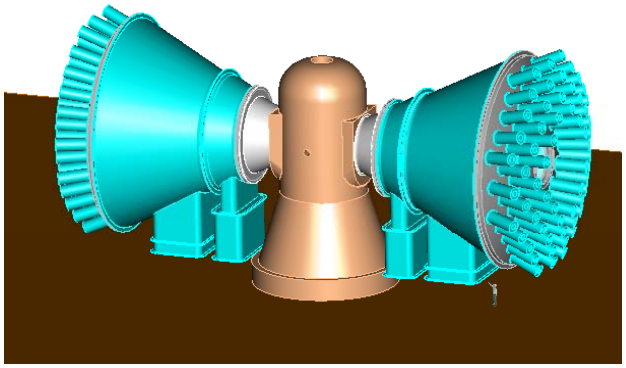

Fig. 3. An isometric view illustrating the coupling of final focus magnet array with the chamber.

We have chosen a set of quadrupole magnets, which, for each beamline, consists of four large-aperture magnets. Block A through E beams all have beamlines in which the final four quadrupoles have the same field strength despite having two distinct energies and a range of perveances. The combined gradient and aperture requirements, the number of channels and the high radiation environment result in a challenging magnet design. Table III gives the field gradient (B'), the beam pipe radius (r_p), field at the pipe radius (B_p) and the magnet length (L). More details are given in [1].

Table III. Final Focus Magnet Parameters

Quad*	B'(T/m)	B_p(T)	r_p(cm)	L(m)
1	21.8	2.61	12.0	1.33
2	-19.1	-3.60	18.9	3.00
3	19.1	3.74	19.6	3.00
4	-21.8	-2.99	13.7	1.33
* Magnet 1 is closest to chamber				

NbTi conductor is used in magnet #1, in order to improve the coil lifetime under heavy radiation load. Nb_3Sn, which allows a better field and temperature margin, is required for magnet #2 based on peak field and operating temperature considerations. Use of Nb_3Sn in magnet #2 results in good critical current margin, but the very large stored energy and associated Lorentz forces require careful design of the mechanical support structure and quench protection system. Details of this design have yet to be worked out. A shell-type ($\cos 2\theta$) configuration is presently assumed, with coil mechanical pre-stress and support provided by thick stainless steel collars. Space budget considerations prevent the use of a support structure based on iron yoke and outer aluminum shell, a design approach adopted in high field Nb_3Sn accelerator magnets to take advantage of thermal contraction differentials between the structural elements [12].

As the beams propagate through the final focus system, the beams will be subject to chromatic and geometric aberrations. Our analytic calculations, together with slice simulations of the WARP code using fully 3D models of the quadrupole magnets in systems similar to the final RPD, indicate that aberrations will give small contributions to the spot size. IBEAM, which embodies

our analytic understanding of the scaling of the aberrations, estimates contributions of 0.6 mm from geometric aberrations and 0.2 mm from chromatic aberrations. Different effects on the final beam spot size add in quadrature. Therefore, the net effect on the final spot from these aberrations is quite small. Most of the increase in the emittance occurs as a result of imperfect neutralization in the chamber and the resulting non-linear space charge forces.

V. RADIATION SHEILDING OF FINAL FOCUS MAGNETS

Radiation transport, shielding, and activation calculations have been completed for RPD and are reported in Ref. 2. The lifetime for the last magnet (#1) is estimated based upon two criteria: a dose limit of 100 MGy to the insulator, and a fast neutron fluence limit of 10^{19} n/cm^2 to the superconductor. The latter criterion assumes NbTi superconductor is used and that room-temperature anneals are performed after a fluence of 3×10^{18} n/cm^2. The annealing process is assumed to provide a 70% damage recovery. Results indicate that the final focus magnets will last for the life of the plant even assuming a more conservative 5 mm standoff between the beams and liquid vortex in the beam tubes. Magnets 2-4, which use NbSn and do not benefit from radiation annealing, are also predicted to last for more than 30 full power years.

Activation calculations have been performed to determine the classification of the waste. The waste disposal rating (WDR) for the coil region magnet #1 exceeds unity, which indicates that the material would not qualify for disposal via shallow land burial. We expect, however, that relatively minor modifications may be sufficient to reduce the WDR to the point at which the material would be classified as Class C waste. The WDR values for the other magnets (#2-4) are less than one.

VI. CHAMBER

The RPD uses a thick-liquid chamber, derived from the HYLIFE-II chamber design [13,14]. The chamber coolant has been selected to be the molten salt flinabe ($LiNaBeF_4$), which has a melting temperature below 350°C and thus can have very low vapor pressure when used at temperatures around 400°C in vortex flow in beam tubes. The RPD uses two-sided target illumination, with beams arranged in 9x9 square arrays at each end of the chamber. Details of the liquid jet configuration in the chamber are given in Ref. 4. The chamber creates a thick-liquid configuration that shields all chamber structures from target neutrons and x-rays. Dumps located in the beam lines between the 3rd and 4th focus magnets, and at the dipole beam bending magnets, absorb the small fraction of neutrons and x rays which propagate up the beam lines.

As illustrated in Fig. 4, the RPD chamber uses three primary types of liquid jets: oscillating jets used to create the central pocket that surrounds the target at the time of ignition, high-precision cylindrical jets that create a square lattice to form the beam ports, and vortices that coat the beam tubes that penetrate the solid shielding and chamber walls. Scaled experiments using water have demonstrated that each of these three jet types can be created [15,16]. For 6.0-Hz operation, the total flow rate is 57 m^3/s with a total pumping power of 27 MWe. The outlet temperature of the bulk flow is 600°C.

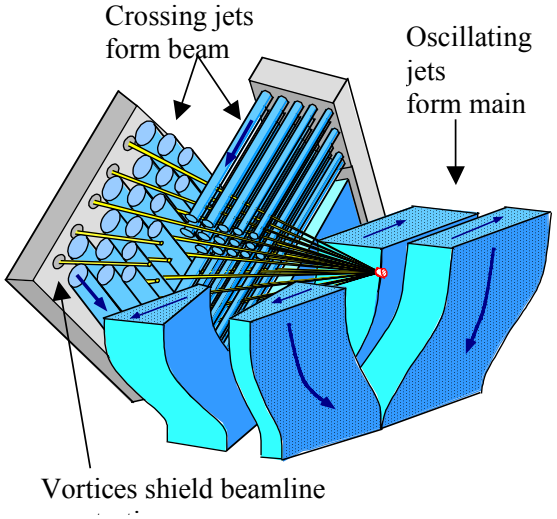

Fig. 4. Illustration of liquid jets required for thick liquid wall chamber.

VII. BEAM NEUTRALIZATION AND MAGNETIC SHUTTER

The end of the last magnet is 6 meters from the target (see Ref. 4 for details). Immediately downstream of the magnet is a 50 cm section consisting of a 20 cm dipole (~ 1 kG) and a 20 cm pulsed plasma source (~10^{13} – 10^{15} /cc). This combination of dipole and pulsed plasma performs the dual function of a plasma plug for beam neutralization and a magnetic shutter for debris removal. The pulsed plasma is timed to provide a 'plasma plug' during the beam entry, and plasma electrons are dragged along by the beam potential for neutralized drift through the next 6 meters to the target. During this phase the dipole magnet inhibits the plasma from moving upstream into the magnetic transport section, where good vacuum is

essential. Another plasma plug is located at chamber entrance for enhanced neutralization after beam transit. The same set-up acts as a magnetic shutter. Debris from the target moves up the beam tube. Most debris reaching the beam tubes condenses on the vortex liquid, while the residual material exiting the vortex is fully ionized by the streaming plasma, and the ionized debris is subsequently swept out of the beam tube by the dipole [4]. The magnetic shutter concept has been modeled with TSUNAMI (gas dynamics) and LSP (plasma effects) [17].

VIII. NEUTRALIZED CHAMBER TRANSPORT

Axisymmetric simulations of beam propagation in the chamber have been made using the particle-in-cell code LSP [18]. The RPD assumes "neutralized ballistic transport," in which the beam space charge is largely neutralized by free electrons from several sources in addition to collisional ionization between beam ions and the background gas. The most effective electron source in these simulations is highly ionized hydrogen plasma injected immediately after the final-focus magnets and also at the location where the beam tube opens into the main chamber (see Ref. 4). The neutralization provided by these plasma layers is enhanced by Child-Langmuir emission from the port wall, which allows the plasma to remain quasi-neutral as electrons are pulled away by the ion beam [19]. In addition, soft x rays from the heated hohlraum ionize the residual gas immediately around the target and help neutralize main pulses and later-arriving foot pulses. Simulations indicate that the optimum plasma density is somewhat greater than the beam density, and no improvement in transport is found for higher densities. A background-gas density of 7×10^{12} cm^{-3} of BeF_2 (the equilibrium vapor pressure [20] of the 600°C flinabe jets used for wall protection) and a chamber radius of 3 m were used in the simulations. We chose a beam convergence angle of 10 mrad, which gives near optimal focusing.

When pre-neutralizing plasmas are used, the simulations give waist radii for Bi^+ foot and main pulses that meet the requirements of the distributed radiator target (see Fig. 5) [21]. Specifically, a main pulse (type E in Table I) has a time-averaged rms radius at its waist of 1.4 mm, and 87% of the beam energy falls within a 1.8-mm radius spot. The initial short foot pulse (Block A in Table 1), which heats the hohlraum to about 100 eV, is more challenging due to the absence of photoionized plasma near the target. In this case, the time-averaged rms radius is 1.7 mm, and about 91% of the beam energy fall inside the required 2.2-mm radius spot. While this result is at best marginal, we find that a substantial part

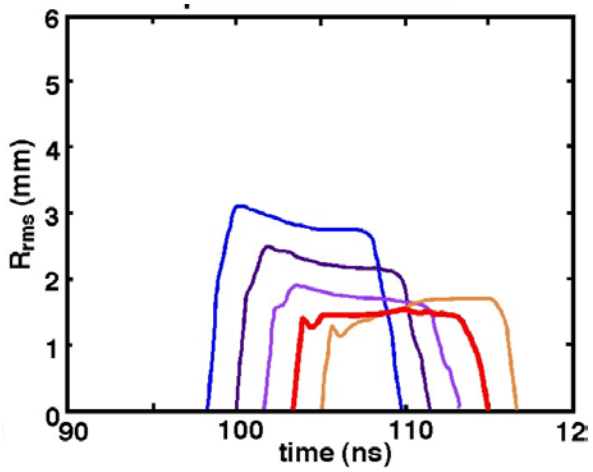

Fig. 5. Time history of rms radius of main pulse beam indicating that 1.8 mm requirement is met.

of the waist radius can be attributed to emittance growth as the beam enters the first plasma layer, resulting from electrons streaming into the beam along the axis and distorting the net space-charge field. This effect can be reduced dramatically by increasing the rise and fall lengths of the plasma and by using magnetic fields to impede electron motion. Effects of the dipole magnet in the magnetic shutter have not been included in the above mentioned code results. With a 6-cm parabolic rise and fall length on the plasma layers, instead of the nominal 3-cm length, the emittance growth is 30% lower, and there is a corresponding drop in the waist radius. We have not simulated the other pulse types (B-D), but previous simulations indicate that the waist radius decreases with decreasing current until it reaches the limit set by the initial emittance. We believe, therefore, that the lower-perveance beams in Table IV can be focused to the required spot without additional difficulty.

The physics model used in these simulations omits some aspects of chamber transport, particularly the target and the molten-salt jets. However, simulations representing the target by an emitting grounded disk show no significant effect on transport, and a simple axisymmetric model, representing the jets by rings of plasma, indicate a modest improvement in transport due to the additional electrons near the beam. Most propagation studies to date model only a single beam, but a few simulations using converging axisymmetric rings of ions to model multiple beams show no significant beam degradation at the waist. Full 3-D simulations are planned to model beam-beam interactions more realistically and to study non-axisymmetric instabilities.

IX. POWER PLANT PARAMETERS AND COE

Table IV summarizes the plant parameters for the RPD. At 6 Hz, the fusion power is 2400 MW, but neutron reactions in the blanket result in a thermal power of 2832 MWt. We envision a multiple-reheat helium Brayton cycle for power conversion cycle with an efficiency of 44% resulting in a total electric power production of 1246 MWe. After accounting for in-plant auxiliary power requirements (4% of gross electric), pumping power of the liquid wall chamber, and the driver power of 110 MWe, the net output of the plant is 1059 MWe. The total cost of the power plant is ~ $5B, with the driver accounting for more than half of that. Using standard fusion community economic modeling assumption and including O&M costs, results in a cost of electricity (COE) of ~ 7.2 ¢/kWeh. Here again we note that RPD-2002 was not optimized in any way for economic performance, and that future studies will focus on reducing costs.

Table IV. Summary of Power Plant Parameters

Driver energy, MJ	7.0
Target gain	57
Target yield, MJ	400
Pulse rep-rate, Hz	6.0
Fusion power, MW	2400
Thermal power, MWt	2832
Conversion efficiency, %	44
Gross electric power, MWe	1246
Auxiliary power, MWe	50
Pumping power, MWe	27
Driver efficiency, %	38
Driver power, MWe	110
Net Electric power, MWe	1058
Driver cost, $B	2.78
Other plant costs, $B	2.27
Total power plant cost, $B	5.05
COE, ¢/kWeh	7.18

Figure 6 shows how the COE varies with driver energy assuming a target gain curve fit through the reference design point. We see that the RPD is very near the minimum COE for the current set of robust assumptions. While operating at a somewhat lower driver energy of ~ 6 MJ would reduce the COE by ~ 3%, the corresponding rep-rate of 8 Hz would require liquid jet injection velocities of >17 m/s, exceeding our currently assumed limit of 12 m/s based on corrosion and erosion concerns.

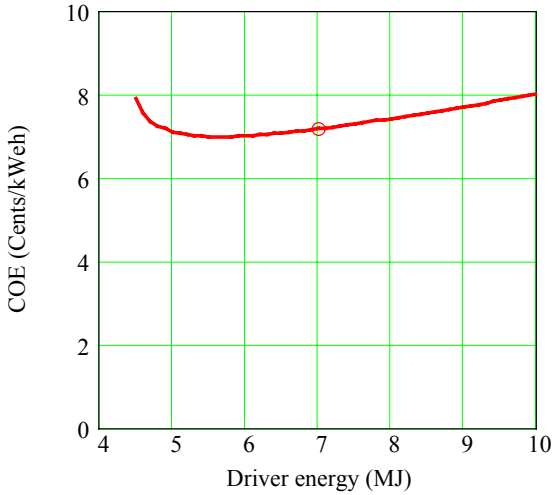

Fig. 6. COE versus driver energy for a fixed 1 GWe plant. The circle indicates the point design.

X. OPPORTUNITIES FOR IMPROVEMENT

We do not believe this study will be the final design of the first heavy ion fusion power plant. We have identified many areas that we did not have time to fully explore, but will undoubtedly lead to simpler, more cost effective designs. These are summarized here.

Target. Higher target gain at lower driver energy than was assumed for the RPD can be achieved in several ways. If the beams can be focused to spots approximately 1 mm in radius, then a "close-coupled" target can be used. 2-D integrated Lasnex calculations of this target show gain of 130 from 3.3 MJ of ion beam energy. Basically, this implies the same yield (and thus the same 1 GWe power plant) with less than half the RPD driver energy. Other opportunities for higher gain at lower driver energy are ion beam direct drive or fast ignition. Both of these options require more work on understanding the relevant target physics.

Driver. The RPD driver uses Bi ions (A=209) in order to give high confidence in beam propagation through the chamber and focusing to the required spot size on target. Our past systems studies of multi-beam heavy drivers have shown a strong economic incentive for moving to lower mass ions such as Xe (A=131), partly because the final ion kinetic energy is lower with lower mass (to keep the same ion range). An additional benefit is that the driver efficiency is higher with lower mass ions for a given total driver energy. If beam focusing can be improved or high gain targets that can accept larger spot sizes prove feasible, moving to a lower mass ion is likely the most significant opportunity for improvement in the driver.

Final Focus Magnets. A possible alternative to the FF magnet configuration described in Ref. 2 is to use clusters of closely packed beams (typically 3x3) with small inter-beam convergence angle. Each cluster is focused by a sub-array of quadrupoles with coils parallel to each other, with the central quad aligned to the central beam axis and the adjacent beams going through their respective channels at an angle. This scheme allows (a) bringing the beam axes in each cluster closer to each other, (b) use of simpler racetrack coils with a common support structure, and (c) use of a separate cryostat for each sub-array. Each sub-array is magnetically decoupled from the others by a flux-return iron yoke. The available beam aperture can accommodate beams traveling at an angle of a few mrad with respect to the magnetic axis, by cutting the inner radiation shields parallel to the beam axes. In the longer term, the demonstration of appropriate performance with high-TC superconductors, operating at liquid-nitrogen temperatures, could have major implications for the RPD final focusing.

Chamber. Currently no experimental or theoretical basis exists to set the limit on the maximum possible repetition rates in thick-liquid chambers, even though the system economics favor somewhat higher repetition rate. Significant improvements in pumping power could come from reducing the array angle, which would reduce the cross-sectional area of the cylindrical jets. These jets have high pumping power requirements, due to the flow conditioning required to suppress turbulence and generate highly smooth surfaces. Higher temperature operation in the main chamber can increase the power cycle thermodynamic efficiency, but also would increase the main-chamber gas density.

Radiation Shielding. In future work on activation, the shielding design will be optimized and trade-offs between insulator and superconductor lifetimes will be conducted. A modification to further emphasize neutron shielding over gamma-ray shielding may reduce the WDR of the coils, while still yielding an acceptable insulator lifetime. Reported results in Section V are averages for each group of magnets, but there is considerable variation within each grouping. Future work will seek to reduce these variations, whether statistical or actual in nature.

Chamber Transport. The LSP calculations to date include an emittance growth at entrance into the plasma plug. We believe that the dipole magnet can remove this growth. We expect that the results including this correction will be substantially improved. This will allow us to go to smaller spots and/or lower mass ions.

XI. SUMMARY AND CONCLUSIONS

We have obtained a point design for a heavy ion fusion power plant that meets all known physics and technology constraints. The driver energy is 7 MJ, with 5.25 MJ from 72 Bi^+ main pulse beams at 4 GeV, and 1.76 MJ from 48 Bi^+ foot beams at 3.3 GeV. This study includes a target that, through detailed simulations, provides a gain of 57. The accelerator has a calculated efficiency of 38%. Operating at 6 Hz, the plant has a net electric power of 1 GWe. The final focusing magnets are shielded by a combination of flowing molten salt jets and vortices, magnetic dipoles and solid shielding material, resulting in lifetimes of 30 years or longer based on 3D particle transport simulations. The superconducting quadrupoles that constitute the final focusing magnets have very large apertures, stored energy and forces, but the fields required have been obtained in other particle accelerators. The final spot size based on our analytic and numerical understanding of neutralized beam transport, meets the target requirements.

ACKNOWLEDGMENTS

Work of LLNL and LBNL authors performed under the auspices of the U.S. Department of Energy by the University of California, Lawrence Livermore National Laboratory under contract No. W-7405-ENG-48 and by Lawrence Berkeley National Laboratory under contract No. AC03-76SF00098.

REFERENCES

1. T. Brown, J. Chun, P. Heitzenroeder, J. Schmidt, "An Integrated Mechanical Design Concept for the Final Focusing Region for the HIF Point Design," these proceedings.
2. J. F. Latkowski, W. R. Meier, "Shielding of the Final Focusing System in the HIF Point Design," these proceedings.
3. S. Pemberton, R. Abbott, P. F. Peterson, "Thick-Liquid Blanket Configuration and Response for the Heavy-Ion Point Design," these proceedings.
4. C.S. Debonnel, S.S. Yu, P.F. Peterson, "X-Ray Ablation and Debris Venting for the HIF Point Design," these proceedings.
5. M. Tabak, D. A. Callahan-Miller, D. D.-M. Ho, G. B. Zimmerman, *Nuclear Fusion*, **38**, 509 (1998).
6. D.A. Callahan-Miller and M. Tabak, *Nuclear Fusion*, **39**, 883 (1999).
7. D.A. Callahan-Miller and M. Tabak, *Phys. of Plasmas*, **7**, 2083 (2000).
8. D.A. Callahan, M.C. Herrmann, M. Tabak, *Laser and Particle Beams, **20**(3) 405* (2002).

9. W. Meier, R. Bangerter, A. Faltens, "An integrated systems model for heavy ion drivers," *Nucl. Inst. and Meth. in Phys. Res. A*, **415**, 249 (1998).
10. W. Meier, R. Bangerter, J. Barnard, "A 3.3 MJ Rb+1 driver design based on an integrated systems analysis," *Nucl. Inst. and Meth. in Phys. Res. A*, **464**, 433 (2001).
11. M. Weber, et al., "Development of a Bi+ source for a heavy-ion driver ignition facility", *Nucl., Inst. And Meth. In Phys. Res. A*, **415,** 339-344, (1998)
12. G. Sabbi, "Status of Nb3Sn Accelerator Magnet R&D," *IEEE Trans. Appl. Supercond.*, **12**, No. 1, 236-241 (March 2002).
13. Moir, R.W., *et al.*, "HYLIFE-II: A Molten-Salt Inertial Fusion Energy Power Plant Design--Final Report," *Fusion Technology*, **25,** 5-25 (1994).
14. P.F. Peterson, "Design Methods for Thick-Liquid Protection of Inertial Fusion Chambers," *Fusion Technology*, **39**, No. 2, 702-710 (2001).
15. R. Abbott, et al., "Cylindrical Liquid Jet Grids for Beam-Port Protection of Thick-Liquid Heavy-Ion Fusion Target Chambers," *Fusion Technology*, **39**, 732-738, (2001).
16. S. Pemberton, C. Jantzen, J. Kuhn, and P.F. Peterson, "Partial-Pocket Experiments for IFE Thick-Liquid Pocket Disruption and Clearing," *Fusion Technology*, **39**, 726-731 (2001).
17. C.S. Debonnel, et al., "Gas Transport and Density Control in the HYLIFE Heavy-Ion Beam Lines", submitted to *Fusion Science and Technology*.
18. D.R. Welch, D. V. Rose, B. V. Oliver, and R. E. Clark, *Nucl. Instrum. Meth. Phys. Res. A*, **464**, 134 (2001).
19. D. R. Welch, D. V. Rose, W. M. Sharp, and S. S. Yu, "Effects of pre-neutralization on heavy-ion fusion chamber transport," to appear in *Lasers and Particle Beams* (2002).
20. D.R. Olander, G. Fukuda and C.F. Baes Jr, "Equilibrium pressures over BeF_2/LiF (flibe) molten mixtures," *Fusion Science and Technology*, **41**, 141-150 (2002).
21. W.M. Sharp et al., "Simulation of Chamber Transport for Heavy Ion Fusion," Proc. 19th IAEA Fusion Energy Conference (Lyon, France, 14-19 Oct. 2002) to appear.